

Unveiling The Quasar Main Sequence: Illuminating The Complexity Of Active Galactic Nuclei And Their Evolution

Swayamtrupta Panda^{1,2,†,*}

¹ *International Gemini Observatory/NSF NOIRLab, Casilla 603, La Serena, Chile*

² *Laboratório Nacional de Astrofísica - MCTI, R. dos Estados Unidos, 154 - Nações, Itajubá - MG, 37504-364, Brazil*

[†] *Gemini Science Fellow*

Correspondence*:

Corresponding Author

swayamtrupta.panda@noirlab.edu

ABSTRACT

The Eigenvector 1 schema, or the main sequence of quasars, was introduced as an analogous scheme to the HR diagram that would allow us to understand the more complex, extended sources - active galactic nuclei (AGNs) that harbor accreting supermassive black holes. The study has spanned more than three decades and has advanced our knowledge of the diversity of Type-1 AGNs from both observational and theoretical aspects. The quasar main sequence, in its simplest form, is the plane between the FWHM of the broad $H\beta$ emission line and the strength of the optical $Fe\text{II}$ emission to the $H\beta$. While the former allows the estimation of the black hole mass, the latter enables direct measurement of the metal content and traces the accretion rate of the AGN. Together, they allow us to track the evolution of AGN in terms of the activity of the central nuclei, its effect on the line-emitting regions surrounding the AGN, and their diversity making them suitable distance indicators to study the expansion of our Universe. This mini-review aims to provide (i) a brief history leading up to the present day in the study of the quasar main sequence, (ii) introduce us to the many possibilities to study AGNs with the main sequence as a guiding tool, and (iii) highlight some recent, exciting lines of researches at the frontier of this ever-growing field.

Keywords: active galactic nuclei; quasars; Seyfert galaxies; emission lines; AGN variability; changing-look AGNs; accretion disks

1 WHAT IS THE QUASAR MAIN SEQUENCE? - A BRIEF HISTORY

More than three decades ago, Boroson and Green (1992) put forward the idea of a main sequence of quasars - an analogous schema to the Hertzsprung-Russell (HR) diagram (Hertzsprung, 1911; Russell, 1914) that has allowed us to track the evolution of stars of varied ages and diverse properties utilizing the classification based on their color and magnitude. Akin to the HR diagram, the quasar main sequence (QMS) was envisioned to help put together the diverse population of Type-1, unobscured active galactic nuclei (AGNs) through the compilation of spectral properties from the broad- and narrow line-emitting regions of a sample of nearby, bright AGNs.

Before diving into the recent advances, we would like to reflect on the importance of Boroson and Green's work with a brief account of the procedure carried out to realize the first results that laid the foundations of the Quasar Main Sequence.

1.1 The inception of the Main Sequence of quasars

Boroson and Green conducted their study within the low-redshift range ($z < 0.5$), analyzing 87 sources from the Bright Quasar Survey (Schmidt and Green, 1983). Their primary finding from optical spectra analysis of these quasars was that the FeII line equivalent width consistently matched that of H β , indicating that FeII emission originates from the same broad-line region (BLR) clouds as H β . Additionally, they compiled optical spectral properties for each source. They integrated these with data from other spectral regions from previous studies, creating a 17-parameter correlation matrix for emission lines and continuum properties. Using principal component analysis (PCA, Francis and Wills 1999) on this matrix to identify meaningful correlations, they focused on 13 key properties including M_V (V-band magnitude), $\log R$ (radio-to-optical spectral index, Kellermann et al. 1989), α_{ox} (optical-to-X-ray spectral index, Tananbaum et al. 1986), EW(H β), [OIII] λ 5007 strength, HeII λ 4686 strength, FeII (4434-4684Å) strength (see also left panel of Figure 1), [OIII] λ 5007/H β peak height ratio, FWHM(H β), H β profile shift, shape, asymmetry, and $M_{[OIII]}$. They determined that the primary eigenvector (Eigenvector 1 or EV1) derived from these properties was primarily characterized by the anti-correlation between FeII strength (specifically R_{FeII} , the ratio of EW(FeII) for the 4434-4684Å blend to EW(H β) and [OIII] λ 5007 strength. EV1 also showed significant correlations ($> |0.5|$) with $\log R$, FWHM(H β), and H β profile asymmetry.

To interpret the PCA results, the authors identified several key parameters that could influence the observed properties: (1) the mass accretion rate, (2) the black hole (BH) mass, (3) the covering factor of the BLR clouds, (4) the degree of anisotropy in the emitted radiation from the continuum source, (5) the orientation of the source to the observer, (6) the velocity distribution of the BLR clouds, and (7) the ionization parameter.

To summarize, the paper by Boroson and Green (1992) is fundamental for two main reasons:

1. It is one of the first publications in AGN research to use principal component analysis (PCA) to explore the connections between the observed properties of quasars, particularly in the study of the Quasar Main Sequence (see right panel of Figure 1 for a recent rendition). This sequence unifies the diverse group of AGNs through Eigenvectors, specifically, Eigenvector 1, which shows an anti-correlation between the width of the optical FeII blend (4434-4684Å) and the peak intensity of the forbidden [OIII] λ 5007Å line. The study also established a connection between the width of the broad H β emission and this eigenvector, forming the well-known "Quasar Main Sequence", primarily driven by the Eddington ratio among other physical properties (e.g., Sulentic et al., 2000; Shen and Ho, 2014; Marziani et al., 2018; Panda et al., 2019c, and references therein).

2. For the first time, the paper constructed the FeII pseudo-continuum template from the optical spectrum of I Zw 1. This template has become widely used in analyzing the optical spectra of AGNs, facilitating the study of the FeII complex (Phillips, 1978a) both theoretically and observationally. It helped understand the excitation mechanisms (Phillips, 1978b; Verner et al., 1999) behind the thousands of spectral transitions from the UV to the NIR, transforming FeII from being considered a spectral contaminant to an evolution tracer and fundamental component of the BLR in AGNs (Marinello et al., 2016; Marziani et al., 2018; Panda et al., 2019c; Martínez-Aldama et al., 2021b; Panda, 2022).

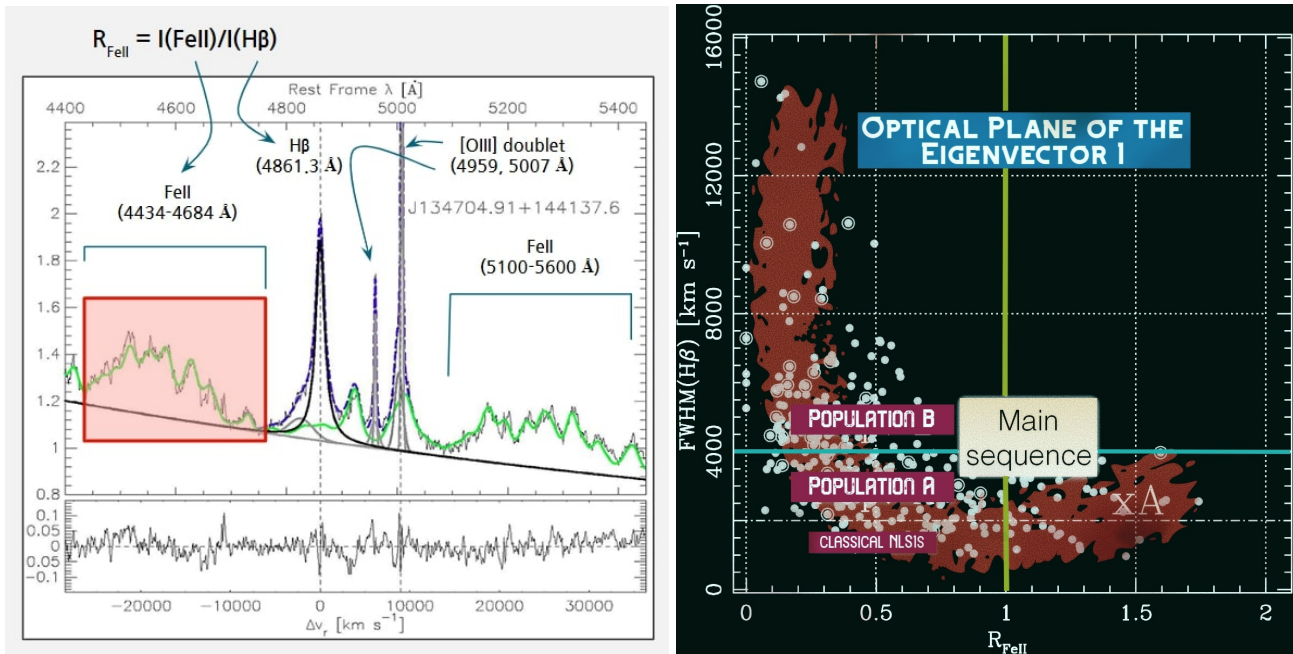


Figure 1. Left: Spectral decomposition (optical region) of a Type-1 Narrow-line Seyfert (NLS1) galaxy, SDSS J134704.91+144137.6. The original spectrum is shown in light gray, the $H\beta$ profile is fit with a Lorentzian function (solid black) and a blue-shifted outflowing component (solid grey), the fit to the $H\beta$ -[O III] complex is shown in dashed gray, and in green the FeII pseudocontinuum fit is shown. The shaded region highlights the FeII blend within 4434-4684 Å used to estimate the FeII strength (wrt broad $H\beta$), i.e., R_{FeII} . The residua from the fit is shown in the bottom panel. Credit: Negrete et al. (2017); **Right:** A Schematic diagram of the optical plane of Eigenvector 1. The solid horizontal line (turquoise) represents the threshold in $\text{FWHM}(H\beta)$ at 4000 km s^{-1} , which distinguishes between Population A and Population B sources (Marziani et al., 2018). The “classical” NLS1s are situated below the $\text{FWHM}(H\beta) \lesssim 2000 \text{ km s}^{-1}$ mark (indicated by the dotted-dashed line). The vertical green line marks the boundary for $R_{\text{FeII}} = 1$, which separates weak from strong FeII emitters, also known as xA sources. Credit: Panda et al. (2024a), Marziani et al. (2018)

1.2 The broad contextualization in the form of 4D Eigenvector 1

An advanced version of the Eigenvector 1 (EV1) schema was introduced by Sulentic et al. (2000), incorporating additional parameters beyond the initial (1) FWHM of the broad component of $H\beta$ and (2) the equivalent width ratio of the optical FeII blend (4434-4684 Å) to broad $H\beta$ (R_{FeII}). These new parameters include (3) the centroid shift at FWHM of the high ionization line C IV $\lambda 1549$, $c(1/2)$, and (4) the soft X-ray photon index (Γ_{soft}). Simplified, these measures: (1) the extent of virialized motions in a low-ionization line-emitting accretion disk or a flattened cloud distribution, acting as a virial estimator of black hole mass (e.g., Collin-Souffrin et al., 1988; Dultzin-Hacyan et al., 1999; Joly et al., 2008) (2) the ionization and size of the BLR cloud, with the FeII emission strength (R_{FeII}) suggesting its origin near the accretion disk; (3) indicators of winds/outflows in high ionization broad line gas; and (4) thermal emission related to the accretion disk and SMBH accretion state (e.g., Mineshige et al., 2000; Done et al., 2012). We refer the readers to a comprehensive summary in Marziani et al. (2018).

Accumulating evidence from subsequent studies, following Boroson and Green (1992), indicates that EV1 correlations involve at least two principal independent parameters: (1) the source’s bolometric luminosity (L_{bol}) and its black hole mass (M_{BH}), convolved with source orientation (Marziani et al., 2001; Panda et al., 2019c). These two parameters are succinctly expressed as the Eddington ratio ($L_{\text{bol}}/L_{\text{Edd}}$).

1.3 Getting the “bigger” picture

The onset of the new century saw the rise of large spectroscopic surveys, such as the Sloan Digital Sky Survey (SDSS, York et al., 2000; Shen et al., 2011). These surveys revitalized EV1 studies and extended their applicability to much larger samples. Shen and Ho (2014) made significant strides with their seminal paper, utilizing data from over 20,000 spectroscopically observed SDSS quasars, analyzed using an automated spectral fitting pipeline (Shen et al., 2011). This study provided spectral parameters for a wide range of emission lines, as well as estimates for black hole masses and Eddington ratios. Leveraging this comprehensive dataset, Shen and Ho redefined the main sequence of quasars and concluded that (1) the average Eddington ratio increases from left to right on the sequence, and (2) the dispersion in FWHM($H\beta$) at a fixed R_{FeII} is largely due to orientation effects (see also Sun and Shen 2015). They proposed that quasar properties correlated with EV1 can be unified by variations in the average Eddington ratio of the accreting black hole, driven by systematic changes in the shape of the accretion disk continuum and its role in photoionizing the line-emitting regions.

More recently, the exploration of large samples has been extended to include sources from the Southern Hemisphere (Chen et al., 2018, and references therein), and the number of Type-1 AGNs, including strong FeII-emitting ones, has grown many folds with deeper surveys extending to fainter magnitudes (Rakshit et al., 2020; Wu and Shen, 2022; Paliya et al., 2024; Panda et al., 2024a). We are now at a stage where AGNs are frequently revisited and thus we also have a wealth of multi-epoch, multi-wavelength data for samples of AGNs. This has greatly helped to build samples of AGNs that demonstrate changes in their continuum and emission line properties - the Changing-Look AGNs (see recent compilations in Panda and Śniegowska, 2024; Guo et al., 2024; Zeltyn et al., 2024, and references therein), especially investigating the changes in the FeII emission in the context of the quasar main sequence (Panda and Śniegowska, 2024).

The paper is organized as follows: In Section 2, we highlight some recent advances in the last decade on the studies with the quasar main sequence - FeII template creation and improvements, theoretical predictions, and advancements in photoionization modeling including some direct confirmations of long-standing hypotheses. We discuss the connection of the main sequence with one of the fundamental properties demonstrated by AGNs - Variability in Section 3, especially in advancing our knowledge through techniques like reverberation mapping (RM), and the renewed interest in Changing-look/Changing-state AGNs. We then give a brief account of the present-day scenario of incorporating AGNs (and quasars) as *standard(izable)* candles and touch upon some relevant studies that have progressed in this direction. Finally, we conclude this mini-review with some closing remarks and perspective for the future in Section 4 with up-and-coming massive, multiplex surveys that will make things more intriguing.

2 QUASAR MAIN SEQUENCE - CURRENT STATE AND ADVANCES

In this section, we touch upon a few of the ongoing, interesting lines of research to improve our understanding of the main sequence of quasars.

2.1 Generating Fe II templates

Owing to its complexity and uncertainties in transition probabilities and excitation mechanisms, the most successful approach to model the FeII emission in AGNs consists of deriving empirical templates from observations and supplementing the missing transitions with state-of-the-art radiative transfer models, e.g. CLOUDY (Ferland et al., 2017; Chatzikos et al., 2023). The templates thus derived using this methodology are referred to as semi-empirical. The work of Kovačević et al. (2010) is seminal in this regard who

provided the AGN community with an interface¹ to create FeII templates by combining the FeII transitions from theoretical expectations and those revealed in the spectrum of the prototypical FeII-emitter, I Zw 1. Their methodology involves the knowledge of the temperature of the ionized cloud responsible for the FeII emission, information on the dynamics of the FeII profile in the observed spectrum, and intensities of the strongest FeII multiplets collected in three groups ($b^4 F$, $a^6 S$, and $a^4 G$). Their semi-empirical templates have been applied to large samples of AGNs, and demonstrated to provide convincing results. All except one went back to the I Zw 1 - in the optical (e.g., Véron-Cetty et al., 2004; Marziani et al., 2021a), in the UV (e.g., Vestergaard and Wilkes, 2001; Bruhweiler and Verner, 2008; Tsuzuki et al., 2006). The exception happened more recently with the HST/STIS observations for Mrk 493 (Park et al., 2022) which has narrower lines, lower reddening, and a less extreme Eddington ratio value than I Zw 1, therefore, can be applied to a larger population of Type-1 AGNs with intrinsically lower FeII emission (Shen and Ho, 2014; Panda et al., 2018). These templates also allow us to infer the velocity information of the FeII emission, a key aspect constraining the geometry and kinematics of the FeII emitting region in the BLR. Studies (Hu et al., 2008; Ferland et al., 2009; Kovačević-Dojčinović and Popović, 2015) have suggested that the FeII emission originates from a location different from, and most likely exterior to, the region that produces most of $H\beta$. These observational findings were confirmed through the analysis of emissivity profiles of AGNs using photoionization modeling (Panda et al., 2018; Sniegowska et al., 2020) and studies of FeII time-lags relative to the $H\beta$ in samples of AGNs using reverberation mapping (Barth et al., 2013; Gaskell et al., 2022).

In recent years, there has been noteworthy development to improve the atomic datasets available for iron emission, with updated radiative and electron collisional rates, and include higher levels (up to 716) and energies as high as 26.4 eV. We refer the readers to Sarkar et al. (2021) for an overview of these datasets and their performance within the spectral synthesis code, CLOUDY.

2.2 FeII spectral synthesis and inferring the BLR cloud properties

Over the years after Boroson and Green put forward their findings from the Eigenvector 1, the expected parameters that should influence the observed correlation in the quasar main sequence have been looked at, albeit separately. Notable among them are (i) the FeII emission model developed in Verner et al. (1999) with 371 atomic levels producing 13,157 (permitted) emission lines with the highest energy level of ~ 11.6 eV; (ii) study by Baldwin et al. (2004) which were among the first to suggest the importance of microturbulence ($\gtrsim 100 \text{ km s}^{-1}$)- the intra-cloud pressure broadening in the broad-line emitting region (BELR) clouds, to explain both the observed shape and equivalent width of the FeII emission. We note that the findings in Baldwin et al. were confined to the UV regime to recover the 2200-2800 Å FeII bump feature. They also suggested the need to include higher metal abundances in the BELR clouds to recover the observed FeII intensities, confirming the earlier results from observations by, e.g., Hamann and Ferland (1993, 1999); Dietrich et al. (2003); (iii) the need to have higher mean densities and column densities in the BELR clouds via numerical modeling to recover the FeII pseudocontinuum behavior, still in the UV regime, was suggested in the paper by Bruhweiler and Verner, who re-affirmed the importance of the microturbulence in the BELR.

In more recent years, a clearer picture of the FeII emission, especially in the optical region, linking to the quasar main sequence has been achieved. There is a growing consensus that the main sequence of quasars, earlier thought to be primarily driven by the Eddington ratio, is in reality, dependent on a combination of parameters of the underlying accretion disk and the BELR clouds Panda et al. (2018, 2019a,c). These

¹ http://servo.aob.rs/FeII_AGN/

parameters are: (1) Eddington ratio, (2) BH mass; (3) shape of the ionizing continuum (SED); (4) BLR density; (5) BLR metallicity; (6) velocity distribution of the BLR clouds (including microturbulence); (7) source's orientation; and (8) BLR cloud sizes (see Panda, 2021a). The 8-dimensional parameter space was first presented by Panda et al. (2019c), and extended by Panda et al. (2020b) wherein through large grids of photoionization models with CLOUDY and massive observational spectroscopic catalogs (Shen et al., 2011; Rakshit et al., 2020) the inherent trends along the main sequence have been confirmed. This almost completes the circle initiated with the hypotheses in Boroson and Green (1992) although more progress is needed, from observational and theoretical aspects. This multi-dimensional parameterization includes the viewing angle to the source (or orientation), which is constrained for a small fraction of the AGNs, especially those that show strong radio “jetted” emissions (see e.g., Padovani et al., 2017, for an overview) or strong water masers (Neufeld et al., 1994; Greenhill et al., 2003). For the remaining sources, the viewing angle is estimated indirectly - through dynamical modeling (Pancoast et al., 2011; Li et al., 2013; Williams et al., 2018; Li et al., 2024), through polarization studies of the emission lines (Savić et al., 2018; Jiang et al., 2021; Śniegowska et al., 2023; Jose et al., 2024), or broad-band SED modeling (Yang et al., 2020; Martínez-Ramírez et al., 2024). The knowledge of the viewing angle is crucial since it can be combined with the spatial and velocity distribution of BLR clouds and their location from the central ionizing source, to estimate the black hole mass of the source. The methodology presented by Panda et al. (2020b) is powerful and acts in dual-purpose - for sources with known orientation and spectroscopically measured FeII emission, it can allow to constrain the BLR density and metallicity. On the other hand, through observed UV diagnostics if the BLR density and metallicity can be inferred (in addition to the FeII emission), one can recover the orientation angle of the source. The methodology, at present, includes the state-of-the-art broad-band SEDs presented in Panda et al. (2019c) and Ferland et al. (2020), while the BH mass, Eddington ratio, velocity distributions and line intensities are from the SDSS QSO catalogs (Shen et al., 2011; Rakshit et al., 2020) for observed AGNs, and can be refined with future multi-wavelength campaigns. Recent works by Pandey et al. (2023, 2024) have extended these results with new, and up-to-date FeII atomic datasets and accounting for dust within the BLR. Additionally, using these new datasets, Dias dos Santos et al. (2023, 2024) have probed into the FeII emission in the NIR regime with the added advantage of transitions being isolated and less in number relative to the optical and UV.

In another recent work (Floris et al., 2024), we performed a multi-component analysis on the strongest UV and optical emission lines and using ~ 10 metal content diagnostic ratios that reveal a systematic progression in metallicity, ranging from sub-solar values to several times higher than solar values. This notable finding was a result of a series of papers (Śniegowska et al., 2021; Garnica et al., 2022; Marziani et al., 2024) wherein a robust recipe of estimating metallicity and other physical parameters in highly-accreting Type-1 AGNs were developed. These results confirm the theoretical predictions made by Panda et al. (2019c) where the increase in the metal content was noted as a key factor that proportionally led to an increase in the FeII emission along the main sequence.

There are multiple studies predating the aforementioned papers that have paved the way to our current understanding of the FeII emission and we recommend the readers to the detailed accounts by e.g., Sulentic et al. (2000); Marziani et al. (2001); Zamfir et al. (2010); D'Onofrio et al. (2012); Shen and Ho (2014); Sulentic and Marziani (2015); Marziani et al. (2018); Gaskell et al. (2022); Panda and Marziani (2023a).

2.3 Developing AGN SEDs along the main sequence

The shape of the ionizing continuum has been an integral part of the main sequence of quasars studies. Around the same time as Boroson and Green, researchers were already developing mean AGN SEDs

(Vanden Berk et al., 2001; Richards et al., 2006), be it to distinguish the sources based on radio dichotomy (Laor et al., 1997) and more recently in Marziani et al. (2021a) or to reveal the prominence of the big blue bump feature in typical Type-1 AGNs (Mathews and Ferland, 1987; Korista et al., 1997). With the advent of large spectroscopic surveys spearheaded by SDSS (York et al., 2000; Shen et al., 2011) AGNs exhibiting stronger FeII emission alike I Zw 1 were being consistently discovered and led to the creation of a mean SED representing Narrow-line Seyfert 1 galaxies (Marziani and Sulentic, 2014). We now have broad-band mean SEDs grouped in Eddington ratios ranging from sub- to super-Eddington limits (Jin et al., 2012, 2017; Ferland et al., 2020). Although these mean SEDs have helped provide statistical inferences on the role of AGN SED in the main sequence trends, having broad-band SED for individual AGNs is a much more recent endeavor that has seen growth. With the increase in simultaneous observations across multiple spectral regimes and the development of self-consistent AGN SED models (Done et al., 2012; Kubota and Done, 2018, 2019; Hagen and Done, 2023), the number of individual sources with broad-band SEDs is growing at a rapid pace, especially for sources demonstrating the most intense FeII emission (Marinello et al., 2020; Jin et al., 2023). Another important extension in the area of SED building is the slim disk AGN SED models (Abramowicz et al., 1988; Wang et al., 2014; Panda and Marziani, 2023b) applicable to those sources accreting at or above the Eddington limit, that show signatures of strong outflows even in the low-ionization emitting regions (e.g., Rodríguez-Ardila et al., 2024).

3 QMS AND AGN VARIABILITY

Another equally important finding was the discovery of the variation in the intensities of emission lines over timescales of weeks to months, suggesting very small emitting regions of the order of a few thousand Schwarzschild radii (Greenstein and Schmidt, 1964). This region is now well-known as the broad-line region (BLR). This crucial discovery opened up a new sub-field called reverberation mapping (RM), which has led to the estimation of black hole masses in hundreds of low- to high-luminosity Seyferts and quasars (Blandford and McKee, 1982; Peterson, 1988, 1993; Peterson et al., 2004), supplemented by single/multi-epoch spectroscopy (Kaspi et al., 2000; Bentz et al., 2013; Du et al., 2016). The BLR's location (R_{BLR}) is closely related to the continuum properties of the underlying accretion disk, with luminosity being the primary observable quantity (Kaspi et al., 2005, and references therein). Subsequent studies, such as Bentz et al. (2013), refined the $H\beta$ -based $R_{\text{BLR}} - L_{5100}$ (or R-L) relation by including more sources and removing the host galaxy's contribution from the total luminosity. Increased monitoring of archival and newer sources has revealed a significant scatter from the empirical R-L relation (Du et al., 2015; Grier et al., 2017; Martínez-Aldama et al., 2019; Du and Wang, 2019; Panda et al., 2019b). This scatter indicates a subset of sources with relatively high luminosities ($\log L_{5100} = 43.0$, in erg s^{-1}) that exhibit shorter time lags and thus shorter R_{BLR} than expected. Recent studies suggest that this scatter may be linked to the accretion rate, providing corrections to the empirical relation based on observables that trace the accretion rate, such as the strength of the optical FeII emission (Du and Wang, 2019; Panda, 2022; Panda and Marziani, 2023a).

On the other hand, the complexity in the modeling and extracting FeII emission from the spectra has led many to search for viable alternatives. Most prominent among the proxy is the Ca II triplet (or CaT) in the NIR given the similarity of the physical conditions required to produce the two ionic species in the BLR (Panda et al., 2020a; Panda, 2021b). In an ongoing series of works (Martínez-Aldama et al., 2015; Marinello et al., 2016; Panda et al., 2020a; Martínez-Aldama et al., 2021b), we have compiled optical FeII and NIR CaT emission strengths and weighed them against each other. We find a robust correlation between the two (Martínez-Aldama et al., 2015; Panda et al., 2020a) primarily driven by the Eddington ratio and in

parts to the BH mass (Martínez-Aldama et al., 2021b). This led us to investigate whether CaT can be a viable replacement for the strength of the FeII emission (or R_{FeII}) in the R-L relation (Martínez-Aldama et al., 2021a). Although the current sample statistics are small in the NIR regime, the spurt of high-quality AGN spectra with the JWST and other ground-based facilities is promising.

3.1 Changing-Look AGNs and our renewed interest in them

Changing-look AGNs have been known for almost as long as the main sequence existed (see recent review by Komossa et al., 2024; Ricci and Trakhtenbrot, 2023). The spectral changes over multiple epochs have now been detected in numerous AGNs - be it extreme variability with the changes in the continuum and emission lines so strong that can be associated with external interference such as obscuration or tidal disruption events (LaMassa et al., 2015; Dodd et al., 2023; Trakhtenbrot et al., 2019), but could very well be associated with intrinsic effects such as disk transition/disk instabilities (Noda and Done, 2018; Ross et al., 2018; Sniegowska et al., 2020) although, the timescales of such events can be widely different (Czerny, 2006).

With the growing interest in finding new changing-look AGNs, the focus has been also to look for AGNs showing variations in their FeII emission (see e.g., Gaskell et al., 2022; Petrushevska et al., 2023). The regular variable nature of AGNs has helped to gain insights into their emitting regions, with some sources where we have estimates of their FeII-emitting locations (see e.g., Hu et al., 2015; Barth et al., 2013) although there are now instances of exceptional changes in the FeII intensities. Panda and Śniegowska (2024) made a compilation of such sources and tracked their transition along the Eigenvector 1 schema and categorized sources that either stay within the same population (A or B, see right panel of Figure 1) or make an inter-population movement as a function of spectral epoch.

3.2 New avenues in Reverberation mapping: BLR saturation and FeII-based R-L relations

In addition to Changing-look AGNs, dedicated spectro-photometric monitoring campaigns on individual sources (e.g., Mrk 6, NGC 5548, NGC 4151, NGC 4051), have allowed us to re-affirm the Pronik-Chuvaev effect i.e., the increase, albeit with a gradual saturation, in the $H\beta$ emitting luminosity with increasing AGN continuum (Pronik and Chuvaev, 1972; Wang et al., 2005; Shapovalova et al., 2008; Gaskell et al., 2021) and more recently in (Panda et al., 2022, 2023a). This assists in building the R-L relation for individual epochs and gaining insights into the temporal behavior of the line-emitting BLR relative to the continuum (Zu et al., 2011; Lu et al., 2022; Feng et al., 2024) although studies to reveal the temporal behavior specifically in FeII are needed to complement the $H\beta$ behavior in these AGNs.

Another interesting revelation has been the construction of the first FeII UV R-L relation in Zajaček et al. (2024b). Here, in addition to improving the existing Mg II-based R-L with 194 sources (more recent compilation in Shen et al. 2024), we have been able to constrain the R-L behavior in UV-emitting FeII for 5 AGNs. The results are motivating as the slope of the R-L is in close agreement with one expected from the standard photoionization theory (i.e., =0.5). Although it is interesting to note that this relation appears steeper than the Mg II R-L relations such that for low-luminosity regimes, the FeII emitting region is closer than the Mg II-emitting region, whereas, at higher luminosities, both relations converge and intersect. This intriguing behaviour needs more explanation which the upcoming RM campaigns may have an answer to. We note that the optical FeII-based R-L relation has been around for some time (see Gaskell et al., 2022, for a recent review). A recent compilation of 17 AGNs (including multiple epoch FeII time lag measurements) from Prince et al. (2023) reveals an R-L for the optical FeII with a slope close to 0.5, and the comparison

with the aforementioned UV-based R-L reveals an offset by a factor of 1.8, i.e., the optical FeII emitting regions are located 1.8 times further out relative to the UV FeII regions.

3.3 Quasars for cosmology: role of the main sequence

Quasars, with their extragalactic origin and persistent bright nature, have long been proposed as “standardizable candles”. With the knowledge of their luminosities (with the aid of the RM and R-L relation) and independently of their fluxes from spectroscopic monitoring, we can determine the luminosity distances of these sources. With a growing number of AGNs (now $\gtrsim 200$, Zajaček et al. 2024b; Shen et al. 2024) where we have such estimates, then allows us to prepare a Hubble diagram - stretching the redshift regime to higher ranges as compared to what we can achieve with other indicators, e.g., Cepheids, Tip of the Red Giant Branch (TRGB), and Type-1a Supernovae (SNIa). We can then scrutinize the various, existing cosmological models, in addition to gauging the performance of quasars to existing indicators, allowing us to link the cosmological measurements from the early Universe (e.g. Planck Collaboration et al. 2020) to the measurements from the late Universe (e.g. Cepheids, SNIa, and TRGBs; Riess et al. 1998, 2019; Freedman et al. 2019).

However, the recent detection of shorter lags in R-L linked to high-accreting sources (Du et al., 2015; Grier et al., 2017; Du et al., 2016) has put the use of R-L relation into uncertainty. In Martínez-Aldama et al. (2019), we looked into the dispersion in the R-L and upon further investigation found the extent of offset of the source’s time-lag is proportional to the Eddington ratio (or more specifically its mass accretion rate). While this helped “standardize” the R-L relation, there remained a circularity problem - the mass accretion rate needs the knowledge of luminosity a priori, and the latter can be estimated assuming a cosmological model. This defeats the purpose of using quasars for cosmology and thus, requires us to find a direct observable parameter that can replace the mass accretion rate. What can be that? In Du and Wang (2019), the authors found that the FeII strength (or R_{FeII}) is a viable alternative to the mass accretion rate (as has been noted in earlier works of Marziani et al. 2018; Panda et al. 2019c) and can correct the dispersion in the R-L. This R_{FeII} -dependent R-L relation has hence been tested and confirmed in other works (Panda, 2022; Panda and Marziani, 2023a). Other empirical relations notably the $L_X - L_{\text{UV}}$ relation, are proposed as a viable alternative to the R-L relation (Risaliti and Lusso, 2015, 2019) although there are subtle differences between the two relations and their inferences. Yet another methodology has been proposed, i.e., with the aid of the existing correlation between the luminosity and the velocity distribution of the BELR (Dultzin et al., 2020; Marziani et al., 2021b), equivalent to the original formulation of the Faber-Jackson law (Faber and Jackson, 1976). We refer the readers to Panda and Marziani (2023a) for more details.

In a parallel direction, efforts to reconcile the use of quasars along with other distance indicators, e.g., SNIa, Gamma-ray bursts, Baryon Acoustic Oscillations, and temperature anisotropy across the microwave background, have been made including the R_{FeII} parameter for the quasar-based R-L relations (Cao et al., 2022; Khadka et al., 2023; Dainotti et al., 2023). Other systematics, such as dust extinction can contribute to and reconcile the observed difference between the R-L and $L_X - L_{\text{UV}}$ relation (Zajaček et al., 2024a). As we enter into the discussions around Hubble-Lemaître law and the H_0 tension, a key to resolving this is better measurements of cosmological distances. VLT/GRAVITY has opened up avenues to probe the angular sizes of the BLR in nearby AGNs using high-resolution spectroastrometry (Gravity Collaboration et al., 2018; GRAVITY Collaboration et al., 2020, 2021, 2024). These angular sizes can be combined with the BLR linear sizes (the latter estimated using the RM technique) to give the parallax distance to these AGNs. The technique was originally conceived in Elvis and Karovska (2002) although thanks to the recent interferometric measurements by GRAVITY coupled with their long-term RM monitoring campaign,

Wang et al. (2020) have been able to estimate, for the first time, a H_0 value using this joint analysis with AGNs. Ongoing improvements with GRAVITY (see e.g., Nowak et al., 2024) will allow the compilation of a sizable sample of AGNs extending to $z \sim 2$ where the spectroastrometric-RM (or, SARM) technique can be applied to build the Hubble diagram for quasars. This however requires the knowledge of the BLR properties that are neatly tied to the quasar main sequence which positively affect the accuracy of the estimation of the cosmological distances to these cosmic objects.

4 CLOSING REMARKS AND FUTURE PERSPECTIVE

FeII emission has been long perceived as a contaminant in the AGN spectra and ways to remove this contamination were sought to enable study and reliable extraction of other emission line properties. The emission turned out to be so useful that a niche of studies linking to the FeII emission was proposed and expanded. To date, the studies stemming from the FeII analysis have crucial contributions in developing our understanding of the line-emitting regions in the BLR leading up to the standardization of quasar-based scaling relations. This mini-review cannot do justice to the enormous literature about the study of FeII emission and its link to the quasar main sequence. Yet, we have tried to touch upon some key aspects in this short overview. We are already in the data-driven astronomy era with multiple facilities working in cohesion, to reveal more connections to the quasar main sequence.

Finally, we glance upon some recent avenues that will have a direct impact on the ongoing studies:

- Ongoing and upcoming spectroscopic surveys such as JWST (Rigby et al., 2023), MSE (Marshall et al., 2019), WST (Mainieri et al., 2024), 4MOST (de Jong et al., 2019) are going to help reveal intriguing FeII signatures in low-luminosity regimes and distant quasars, e.g., JWST ASPIRE (and references therein Yang et al., 2023) showing high FeII emitting AGNs beyond the cosmic noon; putting into question the prevalence of heavy metals in such early epochs. Additionally, the first couple of years of observations with JWST has revealed the numerous faint, broad-line AGN at $z > 5$ (Onoue et al., 2023; Kocevski et al., 2023; Harikane et al., 2023; Matthee et al., 2024; Maiolino et al., 2023; Larson et al., 2023; Greene et al., 2024). A significant fraction of them ($\sim 20\%$) show a steep red continuum in the rest-frame optical region, in addition to being relatively bluer in the UV (Kocevski et al., 2023; Harikane et al., 2023; Matthee et al., 2024; Greene et al., 2024; Killi et al., 2023) giving the appearance of a “V-shape” in the SEDs for these intriguing objects. These sources, also known as “little red dots” (LRDs, Matthee et al., 2024; Kocevski et al., 2024), and while the prominent broad emission lines (i.e., Balmer lines) are relatively easier to deblend. Their profiles can be fitted even under moderate spectral quality, while complex emissions like the FeII would require future deeper observations to check their location on the main sequence of quasars to reveal their nature and chemical history at such redshifts.
- On the other hand, the large-scale photometric surveys (e.g., ZTF: Bellm et al. 2019, LSST: Ivezić et al. 2019, Euclid: Euclid Collaboration et al. 2022) will identify newer AGNs, and combined with the wide-area spectroscopic surveys will allow constraining the FeII contribution and improve our understanding of the various mechanisms involved in FeII production across UV-optical-NIR regime, especially dealing with time-lag recovery and extracting broad-band SED for tens of hundreds of AGNs across a wide range of redshifts (see Panda et al., 2023b, for a recent review).
- With the LSST about to begin its decade-long survey, the use of meter-class ground-based facilities in cohesion with such massive surveys will be pertinent (Chelouche et al., 2019; Panda et al., 2024b); narrow-band filters will allow optimizing the lag-recovery by mitigating spectral windows with

contamination. While, the use of traditional and machine-learning techniques are going to be integral for target selection from erstwhile surveys (Baron, 2019; Sánchez-Sáez et al., 2021; López-Navas et al., 2022; Śniegowska et al., 2023).

CONFLICT OF INTEREST STATEMENT

The author declares that the research was conducted in the absence of any commercial or financial relationships that could be construed as a potential conflict of interest.

AUTHOR CONTRIBUTIONS

SP conceived the idea, designed the layout, collected the data, and wrote and edited the manuscript.

ACKNOWLEDGMENTS

SP acknowledges the financial support of the Conselho Nacional de Desenvolvimento Científico e Tecnológico (CNPq) Fellowships 300936/2023-0 and 301628/2024-6. SP is supported by the international Gemini Observatory, a program of NSF NOIRLab, which is managed by the Association of Universities for Research in Astronomy (AURA) under a cooperative agreement with the U.S. National Science Foundation, on behalf of the Gemini partnership of Argentina, Brazil, Canada, Chile, the Republic of Korea, and the United States of America. This mini-review has been made possible thanks to many past and ongoing collaborations; I would like to thank Bożena Czerny, Paola Marziani, Alberto Rodríguez Ardila, Mary Loli Martínez-Aldama, Murilo Marinello, Marzena Śniegowska, Francisco Pozo-Nuñez, Michal Zajaček, Edi and Nataša Bon, Szymon Kozłowski and many others for their invaluable support, constant motivation and fruitful discussions. I am grateful to the organizers of the “Frontiers in Astronomy and Space Sciences: A Decade of Discovery and Advancement - 10th Anniversary Conference” for the invitation to write this mini-review.

REFERENCES

- Abramowicz, M. A., Czerny, B., Lasota, J. P., and Szuszkiewicz, E. (1988). Slim Accretion Disks. *ApJ* 332, 646. doi:10.1086/166683
- Baldwin, J. A., Ferland, G. J., Korista, K. T., Hamann, F., and LaCluyzé, A. (2004). The Origin of Fe II Emission in Active Galactic Nuclei. *ApJ* 615, 610–624. doi:10.1086/424683
- Baron, D. (2019). Machine Learning in Astronomy: a practical overview. *arXiv e-prints*, arXiv:1904.07248doi:10.48550/arXiv.1904.07248
- Barth, A. J., Pancoast, A., Bennert, V. N., Brewer, B. J., Canalizo, G., Filippenko, A. V., et al. (2013). The Lick AGN Monitoring Project 2011: Fe II Reverberation from the Outer Broad-line Region. *ApJ* 769, 128. doi:10.1088/0004-637X/769/2/128
- Bellm, E. C., Kulkarni, S. R., Graham, M. J., Dekany, R., Smith, R. M., Riddle, R., et al. (2019). The Zwicky Transient Facility: System Overview, Performance, and First Results. *PASP* 131, 018002. doi:10.1088/1538-3873/aaecbe
- Bentz, M. C., Denney, K. D., Grier, C. J., Barth, A. J., Peterson, B. M., Vestergaard, M., et al. (2013). The Low-luminosity End of the Radius-Luminosity Relationship for Active Galactic Nuclei. *ApJ* 767, 149. doi:10.1088/0004-637X/767/2/149
- Blandford, R. D. and McKee, C. F. (1982). Reverberation mapping of the emission line regions of Seyfert galaxies and quasars. *ApJ* 255, 419–439. doi:10.1086/159843

- Boroson, T. A. and Green, R. F. (1992). The Emission-Line Properties of Low-Redshift Quasi-stellar Objects. *ApJS* 80, 109. doi:10.1086/191661
- Bruhweiler, F. and Verner, E. (2008). Modeling Fe II Emission and Revised Fe II (UV) Empirical Templates for the Seyfert 1 Galaxy I Zw 1. *ApJ* 675, 83–95. doi:10.1086/525557
- Cao, S., Zajaček, M., Panda, S., Martínez-Aldama, M. L., Czerny, B., and Ratra, B. (2022). Standardizing reverberation-measured C IV time-lag quasars, and using them with standardized Mg II quasars to constrain cosmological parameters. *MNRAS* 516, 1721–1740. doi:10.1093/mnras/stac2325
- Chatzikos, M., Bianchi, S., Camilloni, F., Chakraborty, P., Gunasekera, C. M., Guzmán, F., et al. (2023). The 2023 Release of Cloudy. *RevMexA&Ap* 59, 327–343. doi:10.22201/ia.01851101p.2023.59.02.12
- Chelouche, D., Pozo Nuñez, F., and Kaspi, S. (2019). Direct evidence of non-disk optical continuum emission around an active black hole. *Nature Astronomy* 3, 251–257. doi:10.1038/s41550-018-0659-x
- Chen, S., Berton, M., La Mura, G., Congiu, E., Cracco, V., Foschini, L., et al. (2018). Probing narrow-line Seyfert 1 galaxies in the southern hemisphere. *A&A* 615, A167. doi:10.1051/0004-6361/201832678
- Collin-Souffrin, S., Dyson, J. E., McDowell, J. C., and Perry, J. J. (1988). The environment of active galactic nuclei - I. A two-component broad emission line model. *MNRAS* 232, 539–550. doi:10.1093/mnras/232.3.539
- Czerny, B. (2006). The Role of the Accretion Disk in AGN Variability. In *AGN Variability from X-Rays to Radio Waves*, eds. C. M. Gaskell, I. M. McHardy, B. M. Peterson, and S. G. Sergeev. vol. 360 of *Astronomical Society of the Pacific Conference Series*, 265
- Dainotti, M. G., Bargiacchi, G., Bogdan, M., Lenart, A. L., Iwasaki, K., Capozziello, S., et al. (2023). Reducing the Uncertainty on the Hubble Constant up to 35% with an Improved Statistical Analysis: Different Best-fit Likelihoods for Type Ia Supernovae, Baryon Acoustic Oscillations, Quasars, and Gamma-Ray Bursts. *ApJ* 951, 63. doi:10.3847/1538-4357/acd63f
- de Jong, R. S., Agertz, O., Berbel, A. A., Aird, J., Alexander, D. A., Amarsi, A., et al. (2019). 4MOST: Project overview and information for the First Call for Proposals. *The Messenger* 175, 3–11. doi:10.18727/0722-6691/5117
- Dias dos Santos, D., Panda, S., Rodríguez-Ardila, A., and Marinello, M. (2023). Modelling the strong Fe II emission: Simultaneous photoionization modelling in optical and NIR. *Boletim da Sociedade Astronomica Brasileira* 34, 295–299
- Dias dos Santos, D., Panda, S., Rodríguez-Ardila, A., and Marinello, M. (2024). Joint Analysis of the Iron Emission in the Optical and Near-Infrared Spectrum of I Zw 1. *Physics* 6, 177–193. doi:10.3390/physics6010013
- Dietrich, M., Hamann, F., Appenzeller, I., and Vestergaard, M. (2003). Fe II/Mg II Emission-Line Ratio in High-Redshift Quasars. *ApJ* 596, 817–829. doi:10.1086/378045
- Dodd, S. A., Nukala, A., Connor, I., Auchettl, K., French, K. D., Law-Smith, J. A. P., et al. (2023). Mid-infrared Outbursts in Nearby Galaxies: Nuclear Obscuration and Connections to Hidden Tidal Disruption Events and Changing-look Active Galactic Nuclei. *ApJL* 959, L19. doi:10.3847/2041-8213/ad1112
- Done, C., Davis, S. W., Jin, C., Blaes, O., and Ward, M. (2012). Intrinsic disc emission and the soft X-ray excess in active galactic nuclei. *MNRAS* 420, 1848–1860. doi:10.1111/j.1365-2966.2011.19779.x
- D’Onofrio, M., Marziani, P., and Sulentic, J. W. (eds.) (2012). *Fifty Years of Quasars: From Early Observations and Ideas to Future Research*, vol. 386 of *Astrophysics and Space Science Library*. doi:10.1007/978-3-642-27564-7
- Du, P., Hu, C., Lu, K.-X., Huang, Y.-K., Cheng, C., Qiu, J., et al. (2015). Supermassive Black Holes with High Accretion Rates in Active Galactic Nuclei. IV. H β Time Lags and Implications for Super-Eddington Accretion. *ApJ* 806, 22. doi:10.1088/0004-637X/806/1/22

- Du, P., Lu, K.-X., Zhang, Z.-X., Huang, Y.-K., Wang, K., Hu, C., et al. (2016). Supermassive Black Holes with High Accretion Rates in Active Galactic Nuclei. V. A New Size-Luminosity Scaling Relation for the Broad-line Region. *ApJ* 825, 126. doi:10.3847/0004-637X/825/2/126
- Du, P. and Wang, J.-M. (2019). The Radius-Luminosity Relationship Depends on Optical Spectra in Active Galactic Nuclei. *ApJ* 886, 42. doi:10.3847/1538-4357/ab4908
- Dultzin, D., Marziani, P., de Diego, J. A., Negrete, C. A., Del Olmo, A., Martínez-Aldama, M. L., et al. (2020). Extreme quasars as distance indicators in cosmology. *Frontiers in Astronomy and Space Sciences* 6, 80. doi:10.3389/fspas.2019.00080
- Dultzin-Hacyan, D., Taniguchi, Y., and Uranga, L. (1999). Where is the Ca II Triplet Emitting Region in AGN? In *Structure and Kinematics of Quasar Broad Line Regions*, eds. C. M. Gaskell, W. N. Brandt, M. Dietrich, D. Dultzin-Hacyan, and M. Eracleous. vol. 175 of *Astronomical Society of the Pacific Conference Series*, 303
- Elvis, M. and Karovska, M. (2002). Quasar Parallax: A Method for Determining Direct Geometrical Distances to Quasars. *ApJL* 581, L67–L70. doi:10.1086/346015
- Euclid Collaboration, Scaramella, R., Amiaux, J., Mellier, Y., Burigana, C., Carvalho, C. S., et al. (2022). Euclid preparation. I. The Euclid Wide Survey. *A&A* 662, A112. doi:10.1051/0004-6361/202141938
- Faber, S. M. and Jackson, R. E. (1976). Velocity dispersions and mass-to-light ratios for elliptical galaxies. *ApJ* 204, 668–683. doi:10.1086/154215
- Feng, H.-C., Li, S.-S., Bai, J. M., Liu, H. T., Lu, K.-X., Pang, Y.-X., et al. (2024). Velocity-resolved Reverberation Mapping of Changing-look Active Galactic Nucleus NGC 4151 during Outburst Stage. II. Four Season Observation Results. *arXiv e-prints*, arXiv:2409.01637
- Ferland, G. J., Chatzikos, M., Guzmán, F., Lykins, M. L., van Hoof, P. A. M., Williams, R. J. R., et al. (2017). The 2017 Release Cloudy. *RevMexA&Ap* 53, 385–438. doi:10.48550/arXiv.1705.10877
- Ferland, G. J., Done, C., Jin, C., Landt, H., and Ward, M. J. (2020). State-of-the-art AGN SEDs for photoionization models: BLR predictions confront the observations. *MNRAS* 494, 5917–5922. doi:10.1093/mnras/staa1207
- Ferland, G. J., Hu, C., Wang, J.-M., Baldwin, J. A., Porter, R. L., van Hoof, P. A. M., et al. (2009). Implications of Infalling Fe II-Emitting Clouds in Active Galactic Nuclei: Anisotropic Properties. *ApJL* 707, L82–L86. doi:10.1088/0004-637X/707/1/L82
- Floris, A., Marziani, P., Panda, S., Sniegowska, M., D’Onofrio, M., Deconto-Machado, A., et al. (2024). Chemical abundances along the quasar main sequence. *arXiv e-prints*, arXiv:2405.04456doi:10.48550/arXiv.2405.04456
- Francis, P. J. and Wills, B. J. (1999). Introduction to Principal Components Analysis. In *Quasars and Cosmology*, eds. G. Ferland and J. Baldwin. vol. 162 of *Astronomical Society of the Pacific Conference Series*, 363. doi:10.48550/arXiv.astro-ph/9905079
- Freedman, W. L., Madore, B. F., Hatt, D., Hoyt, T. J., Jang, I. S., Beaton, R. L., et al. (2019). The Carnegie-Chicago Hubble Program. VIII. An Independent Determination of the Hubble Constant Based on the Tip of the Red Giant Branch. *ApJ* 882, 34. doi:10.3847/1538-4357/ab2f73
- Garnica, K., Negrete, C. A., Marziani, P., Dultzin, D., Śniegowska, M., and Panda, S. (2022). High metal content of highly accreting quasars: Analysis of an extended sample. *A&A* 667, A105. doi:10.1051/0004-6361/202142837
- Gaskell, C. M., Bartel, K., Deffner, J. N., and Xia, I. (2021). Anomalous broad-line region responses to continuum variability in active galactic nuclei - I. H β variability. *MNRAS* 508, 6077–6091. doi:10.1093/mnras/stab2443

- Gaskell, M., Thakur, N., Tian, B., and Saravanan, A. (2022). Fe II emission in active galactic nuclei. *Astronomische Nachrichten* 343, e210112. doi:10.1002/asna.20210112
- GRAVITY Collaboration, Amorim, A., Bauböck, M., Brandner, W., Bolzer, M., Clénet, Y., et al. (2021). The central parsec of NGC 3783: a rotating broad emission line region, asymmetric hot dust structure, and compact coronal line region. *A&A* 648, A117. doi:10.1051/0004-6361/202040061
- GRAVITY Collaboration, Amorim, A., Bauböck, M., Brandner, W., Clénet, Y., Davies, R., et al. (2020). The spatially resolved broad line region of IRAS 09149-6206. *A&A* 643, A154. doi:10.1051/0004-6361/202039067
- GRAVITY Collaboration, Amorim, A., Bourdarot, G., Brandner, W., Cao, Y., Clénet, Y., et al. (2024). The size-luminosity relation of local active galactic nuclei from interferometric observations of the broad-line region. *A&A* 684, A167. doi:10.1051/0004-6361/202348167
- Gravity Collaboration, Sturm, E., Dexter, J., Pfuhl, O., Stock, M. R., Davies, R. I., et al. (2018). Spatially resolved rotation of the broad-line region of a quasar at sub-parsec scale. *Nat* 563, 657–660. doi:10.1038/s41586-018-0731-9
- Greene, J. E., Labbe, I., Goulding, A. D., Furtak, L. J., Chemerynska, I., Kokorev, V., et al. (2024). UNCOVER Spectroscopy Confirms the Surprising Ubiquity of Active Galactic Nuclei in Red Sources at $z \lesssim 5$. *ApJ* 964, 39. doi:10.3847/1538-4357/ad1e5f
- Greenhill, L. J., Kondratko, P. T., Lovell, J. E. J., Kuiper, T. B. H., Moran, J. M., Jauncey, D. L., et al. (2003). The Discovery of H₂O Maser Emission in Seven Active Galactic Nuclei and at High Velocities in the Circinus Galaxy. *ApJL* 582, L11–L14. doi:10.1086/367602
- Greenstein, J. L. and Schmidt, M. (1964). The Quasi-Stellar Radio Sources 3C 48 and 3C 273. *ApJ* 140, 1. doi:10.1086/147889
- Grier, C. J., Trump, J. R., Shen, Y., Horne, K., Kinemuchi, K., McGreer, I. D., et al. (2017). The Sloan Digital Sky Survey Reverberation Mapping Project: H α and H β Reverberation Measurements from First-year Spectroscopy and Photometry. *ApJ* 851, 21. doi:10.3847/1538-4357/aa98dc
- Guo, W.-J., Zou, H., Greenwell, C. L., Alexander, D. M., Fawcett, V. A., Pan, Z., et al. (2024). Changing-look Active Galactic Nuclei from the Dark Energy Spectroscopic Instrument. II. Statistical Properties from the First Data Release. *arXiv e-prints*, arXiv:2408.00402doi:10.48550/arXiv.2408.00402
- Hagen, S. and Done, C. (2023). Estimating black hole spin from AGN SED fitting: the impact of general-relativistic ray tracing. *MNRAS* 525, 3455–3467. doi:10.1093/mnras/stad2499
- Hamann, F. and Ferland, G. (1993). The Chemical Evolution of QSOs and the Implications for Cosmology and Galaxy Formation. *ApJ* 418, 11. doi:10.1086/173366
- Hamann, F. and Ferland, G. (1999). Elemental Abundances in Quasistellar Objects: Star Formation and Galactic Nuclear Evolution at High Redshifts. *ARA&Ap* 37, 487–531. doi:10.1146/annurev.astro.37.1.487
- Harikane, Y., Zhang, Y., Nakajima, K., Ouchi, M., Isobe, Y., Ono, Y., et al. (2023). A JWST/NIRSpec First Census of Broad-line AGNs at $z = 4-7$: Detection of 10 Faint AGNs with $M_{BH} 10^6-10^8 M_{\odot}$ and Their Host Galaxy Properties. *ApJ* 959, 39. doi:10.3847/1538-4357/ad029e
- Hertzprung, E. (1911). Ueber die Verwendung photographischer effektiver Wellenlaengen zur Bestimmung von Farbaequivalenten. *Publikationen des Astrophysikalischen Observatoriums zu Potsdam* 63
- Hu, C., Du, P., Lu, K.-X., Li, Y.-R., Wang, F., Qiu, J., et al. (2015). Supermassive Black Holes with High Accretion Rates in Active Galactic Nuclei. III. Detection of Fe II Reverberation in Nine Narrow-line Seyfert 1 Galaxies. *ApJ* 804, 138. doi:10.1088/0004-637X/804/2/138

- Hu, C., Wang, J.-M., Ho, L. C., Chen, Y.-M., Zhang, H.-T., Bian, W.-H., et al. (2008). A Systematic Analysis of Fe II Emission in Quasars: Evidence for Inflow to the Central Black Hole. *ApJ* 687, 78–96. doi:10.1086/591838
- Ivezić, Ž., Kahn, S. M., Tyson, J. A., Abel, B., Acosta, E., Allsman, R., et al. (2019). LSST: From Science Drivers to Reference Design and Anticipated Data Products. *ApJ* 873, 111. doi:10.3847/1538-4357/ab042c
- Jiang, B.-W., Marziani, P., Savić, D., Shablovinskaya, E., Popović, L. Č., Afanasiev, V. L., et al. (2021). Linear spectropolarimetric analysis of Fairall 9 with VLT/FORS2. *MNRAS* 508, 79–99. doi:10.1093/mnras/stab2273
- Jin, C., Done, C., Ward, M., and Gardner, E. (2017). Super-Eddington QSO RX J0439.6-5311 - II. Multiwavelength constraints on the global structure of the accretion flow. *MNRAS* 471, 706–721. doi:10.1093/mnras/stx1634
- Jin, C., Done, C., Ward, M., Panessa, F., Liu, B., and Liu, H.-Y. (2023). The extreme super-eddington NLS1 RX J0134.2-4258 - II. A weak-line Seyfert linking to the weak-line quasar. *MNRAS* 518, 6065–6082. doi:10.1093/mnras/stac3513
- Jin, C., Ward, M., and Done, C. (2012). A combined optical and X-ray study of unobscured type 1 active galactic nuclei - III. Broad-band SED properties. *MNRAS* 425, 907–929. doi:10.1111/j.1365-2966.2012.21272.x
- Joly, M., Véron-Cetty, M., and Véron, P. (2008). Fe II emission in AGN. In *Revista Mexicana de Astronomia y Astrofisica Conference Series*. vol. 32 of *Revista Mexicana de Astronomia y Astrofisica Conference Series*, 59–61
- Jose, J., Rakshit, S., Panda, S., Woo, J.-H., Stalin, C. S., Neha, S., et al. (2024). Spectropolarimetric view of the gamma-ray emitting NLS1 1H0323 + 342. *MNRAS* 532, 3187–3197. doi:10.1093/mnras/stae1691
- Kaspi, S., Maoz, D., Netzer, H., Peterson, B. M., Vestergaard, M., and Jannuzi, B. T. (2005). The Relationship between Luminosity and Broad-Line Region Size in Active Galactic Nuclei. *ApJ* 629, 61–71. doi:10.1086/431275
- Kaspi, S., Smith, P. S., Netzer, H., Maoz, D., Jannuzi, B. T., and Giveon, U. (2000). Reverberation Measurements for 17 Quasars and the Size-Mass-Luminosity Relations in Active Galactic Nuclei. *ApJ* 533, 631–649. doi:10.1086/308704
- Kellermann, K. I., Sramek, R., Schmidt, M., Shaffer, D. B., and Green, R. (1989). VLA Observations of Objects in the Palomar Bright Quasar Survey. *AJ* 98, 1195. doi:10.1086/115207
- Khadka, N., Zajaček, M., Prince, R., Panda, S., Czerny, B., Martínez-Aldama, M. L., et al. (2023). Quasar UV/X-ray relation luminosity distances are shorter than reverberation-measured radius-luminosity relation luminosity distances. *MNRAS* 522, 1247–1264. doi:10.1093/mnras/stad1040
- Killi, M., Watson, D., Brammer, G., McPartland, C., Antwi-Danso, J., Newshore, R., et al. (2023). Deciphering the JWST spectrum of a 'little red dot' at $z \sim 4.53$: An obscured AGN and its star-forming host. *arXiv e-prints*, arXiv:2312.03065doi:10.48550/arXiv.2312.03065
- Kocevski, D. D., Finkelstein, S. L., Barro, G., Taylor, A. J., Calabrò, A., Laloux, B., et al. (2024). The Rise of Faint, Red AGN at $z > 4$: A Sample of Little Red Dots in the JWST Extragalactic Legacy Fields. *arXiv e-prints*, arXiv:2404.03576doi:10.48550/arXiv.2404.03576
- Kocevski, D. D., Onoue, M., Inayoshi, K., Trump, J. R., Arrabal Haro, P., Grazian, A., et al. (2023). Hidden Little Monsters: Spectroscopic Identification of Low-mass, Broad-line AGNs at $z \lesssim 5$ with CEERS. *ApJL* 954, L4. doi:10.3847/2041-8213/ace5a0

- Komossa, S., Grupe, D., Marziani, P., Popovic, L. C., Marceta-Mandic, S., Bon, E., et al. (2024). The extremes of AGN variability: outbursts, deep fades, changing looks, exceptional spectral states, and semi-periodicities. *arXiv e-prints*, arXiv:2408.00089doi:10.48550/arXiv.2408.00089
- Korista, K., Baldwin, J., Ferland, G., and Verner, D. (1997). An Atlas of Computed Equivalent Widths of Quasar Broad Emission Lines. *ApJS* 108, 401–415. doi:10.1086/312966
- Kovačević, J., Popović, L. Č., and Dimitrijević, M. S. (2010). Analysis of Optical Fe II Emission in a Sample of Active Galactic Nucleus Spectra. *ApJS* 189, 15–36. doi:10.1088/0067-0049/189/1/15
- Kovačević-Dojčinović, J. and Popović, L. Č. (2015). The Connections Between the UV and Optical Fe II Emission Lines in Type 1 AGNs. *ApJS* 221, 35. doi:10.1088/0067-0049/221/2/35
- Kubota, A. and Done, C. (2018). A physical model of the broad-band continuum of AGN and its implications for the UV/X relation and optical variability. *MNRAS* 480, 1247–1262. doi:10.1093/mnras/sty1890
- Kubota, A. and Done, C. (2019). Modelling the spectral energy distribution of super-Eddington quasars. *MNRAS* 489, 524–533. doi:10.1093/mnras/stz2140
- LaMassa, S. M., Cales, S., Moran, E. C., Myers, A. D., Richards, G. T., Eracleous, M., et al. (2015). The Discovery of the First “Changing Look” Quasar: New Insights Into the Physics and Phenomenology of Active Galactic Nucleus. *ApJ* 800, 144. doi:10.1088/0004-637X/800/2/144
- Laor, A., Fiore, F., Elvis, M., Wilkes, B. J., and McDowell, J. C. (1997). The Soft X-Ray Properties of a Complete Sample of Optically Selected Quasars. II. Final Results. *ApJ* 477, 93–113. doi:10.1086/303696
- Larson, R. L., Finkelstein, S. L., Kocevski, D. D., Hutchison, T. A., Trump, J. R., Arrabal Haro, P., et al. (2023). A CEERS Discovery of an Accreting Supermassive Black Hole 570 Myr after the Big Bang: Identifying a Progenitor of Massive $z \lesssim 6$ Quasars. *ApJL* 953, L29. doi:10.3847/2041-8213/ace619
- Li, Y.-R., Hu, C., Yao, Z.-H., Chen, Y.-J., Bai, H.-R., Yang, S., et al. (2024). Spectroastrometry and Reverberation Mapping (SARM) of Active Galactic Nuclei. I. The $H\beta$ Broad-line Region Structure and Black Hole Mass of Five Quasars. *arXiv e-prints*, arXiv:2407.08120doi:10.48550/arXiv.2407.08120
- Li, Y.-R., Wang, J.-M., Ho, L. C., Du, P., and Bai, J.-M. (2013). A Bayesian Approach to Estimate the Size and Structure of the Broad-line Region in Active Galactic Nuclei Using Reverberation Mapping Data. *ApJ* 779, 110. doi:10.1088/0004-637X/779/2/110
- López-Navas, E., Martínez-Aldama, M. L., Bernal, S., Sánchez-Sáez, P., Arévalo, P., Graham, M. J., et al. (2022). Confirming new changing-look AGNs discovered through optical variability using a random forest-based light-curve classifier. *MNRAS* 513, L57–L62. doi:10.1093/mnras/ltac033
- Lu, K.-X., Bai, J.-M., Wang, J.-M., Hu, C., Li, Y.-R., Du, P., et al. (2022). Supermassive Black Hole and Broad-line Region in NGC 5548: Results from Five-season Reverberation Mapping. *ApJS* 263, 10. doi:10.3847/1538-4365/ac94d3
- Mainieri, V., Anderson, R. I., Brinchmann, J., Cimatti, A., Ellis, R. S., Hill, V., et al. (2024). The Wide-field Spectroscopic Telescope (WST) Science White Paper. *arXiv e-prints*, arXiv:2403.05398doi:10.48550/arXiv.2403.05398
- Maiolino, R., Scholtz, J., Curtis-Lake, E., Carniani, S., Baker, W., de Graaff, A., et al. (2023). JADES. The diverse population of infant Black Holes at $4 < z < 11$: merging, tiny, poor, but mighty. *arXiv e-prints*, arXiv:2308.01230doi:10.48550/arXiv.2308.01230
- Marinello, M., Rodríguez-Ardila, A., Garcia-Rissmann, A., Sigut, T. A. A., and Pradhan, A. K. (2016). The Fe II Emission in Active Galactic Nuclei: Excitation Mechanisms and Location of the Emitting Region. *ApJ* 820, 116. doi:10.3847/0004-637X/820/2/116
- Marinello, M., Rodríguez-Ardila, A., Marziani, P., Sigut, A., and Pradhan, A. (2020). Panchromatic properties of the extreme Fe II emitter PHL 1092. *MNRAS* 494, 4187–4202. doi:10.1093/mnras/staa934

- Marshall, J., Bolton, A., Bullock, J., Burgasser, A., Chambers, K., DePoy, D., et al. (2019). The Maunakea Spectroscopic Explorer. In *Bulletin of the American Astronomical Society*. vol. 51, 126. doi:10.48550/arXiv.1907.07192
- Martínez-Aldama, M. L., Czerny, B., Kawka, D., Karas, V., Panda, S., Zajaček, M., et al. (2019). Can Reverberation-measured Quasars Be Used for Cosmology? *ApJ* 883, 170. doi:10.3847/1538-4357/ab3728
- Martínez-Aldama, M. L., Dultzin, D., Marziani, P., Sulentic, J. W., Bressan, A., Chen, Y., et al. (2015). O I and Ca II Observations in Intermediate Redshift Quasars. *ApJS* 217, 3. doi:10.1088/0067-0049/217/1/3
- Martínez-Aldama, M. L., Panda, S., and Czerny, B. (2021a). A New Radius-Luminosity Relation: Using the Near-Infrared CaII Triplet. In *XIX Serbian Astronomical Conference*. vol. 100, 287–293
- Martínez-Aldama, M. L., Panda, S., Czerny, B., Marinello, M., Marziani, P., and Dultzin, D. (2021b). The CaFe Project: Optical Fe II and Near-infrared Ca II Triplet Emission in Active Galaxies. II. The Driver(s) of the Ca II and Fe II and Its Potential Use as a Chemical Clock. *ApJ* 918, 29. doi:10.3847/1538-4357/ac03b6
- Martínez-Ramírez, L. N., Calistro Rivera, G., Lusso, E., Bauer, F. E., Nardini, E., Buchner, J., et al. (2024). AGNfitter-rx: Modelling the radio-to-X-ray SEDs of AGNs. *arXiv e-prints*, arXiv:2405.12111doi:10.48550/arXiv.2405.12111
- Marziani, P., Berton, M., Panda, S., and Bon, E. (2021a). Optical Singly-Ionized Iron Emission in Radio-Quiet and Relativistically Jetted Active Galactic Nuclei. *Universe* 7, 484. doi:10.3390/universe7120484
- Marziani, P., Dultzin, D., del Olmo, A., D’Onofrio, M., de Diego, J. A., Stirpe, G. M., et al. (2021b). The quasar main sequence and its potential for cosmology. In *Nuclear Activity in Galaxies Across Cosmic Time*, eds. M. Pović, P. Marziani, J. Masegosa, H. Netzer, S. H. Negu, and S. B. Tessema. vol. 356 of *IAU Symposium*, 66–71. doi:10.1017/S1743921320002598
- Marziani, P., Dultzin, D., Sulentic, J. W., Del Olmo, A., Negrete, C. A., Martínez-Aldama, M. L., et al. (2018). A main sequence for quasars. *Frontiers in Astronomy and Space Sciences* 5, 6. doi:10.3389/fspas.2018.00006
- Marziani, P., Floris, A., Deconto-Machado, A., Panda, S., Sniegowska, M., Garnica, K., et al. (2024). From Sub-Solar to Super-Solar Chemical Abundances along the Quasar Main Sequence. *Physics* 6, 216–236. doi:10.3390/physics6010016
- Marziani, P. and Sulentic, J. W. (2014). Highly accreting quasars: sample definition and possible cosmological implications. *MNRAS* 442, 1211–1229. doi:10.1093/mnras/stu951
- Marziani, P., Sulentic, J. W., Zwitter, T., Dultzin-Hacyan, D., and Calvani, M. (2001). Searching for the Physical Drivers of the Eigenvector 1 Correlation Space. *ApJ* 558, 553–560. doi:10.1086/322286
- Mathews, W. G. and Ferland, G. J. (1987). What Heats the Hot Phase in Active Nuclei? *ApJ* 323, 456. doi:10.1086/165843
- Matthee, J., Naidu, R. P., Brammer, G., Chisholm, J., Eilers, A.-C., Goulding, A., et al. (2024). Little Red Dots: An Abundant Population of Faint Active Galactic Nuclei at $z \sim 5$ Revealed by the EIGER and FRESCO JWST Surveys. *ApJ* 963, 129. doi:10.3847/1538-4357/ad2345
- Mineshige, S., Kawaguchi, T., Takeuchi, M., and Hayashida, K. (2000). Slim-Disk Model for Soft X-Ray Excess and Variability of Narrow-Line Seyfert 1 Galaxies. *PASJ* 52, 499–508. doi:10.1093/pasj/52.3.499
- Negrete, C. A., Dultzin, D., Marziani, P., Sulentic, J. W., Esparza-Arredondo, D., Martínez-Aldama, M. L., et al. (2017). Quasars as Cosmological Standard Candles. *Frontiers in Astronomy and Space Sciences* 4, 59. doi:10.3389/fspas.2017.00059
- Neufeld, D. A., Maloney, P. R., and Conger, S. (1994). Water maser emission from X-ray-heated circumnuclear gas in active galaxies. *ApJL* 436, L127–L130. doi:10.1086/187649

- Noda, H. and Done, C. (2018). Explaining changing-look AGN with state transition triggered by rapid mass accretion rate drop. *MNRAS* 480, 3898–3906. doi:10.1093/mnras/sty2032
- Nowak, M., Lacour, S., Abuter, R., Woillez, J., Dembet, R., Bordoni, M. S., et al. (2024). Upgrading the GRAVITY fringe tracker for GRAVITY+. Tracking the white-light fringe in the non-observable optical path length state-space. *A&A* 684, A184. doi:10.1051/0004-6361/202348771
- Onoue, M., Inayoshi, K., Ding, X., Li, W., Li, Z., Molina, J., et al. (2023). A Candidate for the Least-massive Black Hole in the First 1.1 Billion Years of the Universe. *ApJL* 942, L17. doi:10.3847/2041-8213/aca9d3
- Padovani, P., Alexander, D. M., Assef, R. J., De Marco, B., Giommi, P., Hickox, R. C., et al. (2017). Active galactic nuclei: what's in a name? *Astronomy & Astrophysics Reviews* 25, 2. doi:10.1007/s00159-017-0102-9
- Paliya, V. S., Stalin, C. S., Domínguez, A., and Saikia, D. J. (2024). Narrow-line Seyfert 1 galaxies in Sloan Digital Sky Survey: a new optical spectroscopic catalogue. *MNRAS* 527, 7055–7069. doi:10.1093/mnras/stad3650
- Pancoast, A., Brewer, B. J., and Treu, T. (2011). Geometric and Dynamical Models of Reverberation Mapping Data. *ApJ* 730, 139. doi:10.1088/0004-637X/730/2/139
- Panda, S. (2021a). *Physical Conditions in the Broad-line Regions of Active Galaxies*. Ph.D. thesis, Polish Academy of Sciences, Institute of Physics
- Panda, S. (2021b). The CaFe project: Optical Fe II and near-infrared Ca II triplet emission in active galaxies: simulated EWs and the co-dependence of cloud size and metal content. *A&A* 650, A154. doi:10.1051/0004-6361/202140393
- Panda, S. (2022). Parameterizing the AGN Radius–Luminosity Relation from the Eigenvector 1 Viewpoint. *Frontiers in Astronomy and Space Sciences* 9, 850409. doi:10.3389/fspas.2022.850409
- Panda, S., Bon, E., Marziani, P., and Bon, N. (2022). Taming the derivative: Diagnostics of the continuum and H β emission in a prototypical Population B active galaxy. *Astronomische Nachrichten* 343, e210091. doi:10.1002/asna.20210091
- Panda, S., Bon, E., Marziani, P., and Bon, N. (2023a). Saturation of the curve: Diagnostics of the continuum and H β emission in Population B active galaxy NGC 5548. *Boletim da Sociedade Astronômica Brasileira* 34, 246–250. doi:10.48550/arXiv.2308.05831
- Panda, S., Czerny, B., Adhikari, T. P., Hryniewicz, K., Wildy, C., Kuraszkiwicz, J., et al. (2018). Modeling of the Quasar Main Sequence in the Optical Plane. *ApJ* 866, 115. doi:10.3847/1538-4357/aae209
- Panda, S., Czerny, B., Done, C., and Kubota, A. (2019a). CLOUDY View of the Warm Corona. *ApJ* 875, 133. doi:10.3847/1538-4357/ab11cb
- Panda, S., Kozłowski, S., Gromadzki, M., Wrona, M., Iwanek, P., Udalski, A., et al. (2024a). Virial Black Hole Masses for Active Galactic Nuclei behind the Magellanic Clouds. *ApJS* 272, 11. doi:10.3847/1538-4365/ad3549
- Panda, S., Martínez-Aldama, M. L., Marinello, M., Czerny, B., Marziani, P., and Dultzin, D. (2020a). The CaFe Project: Optical Fe II and Near-infrared Ca II Triplet Emission in Active Galaxies. I. Photoionization Modeling. *ApJ* 902, 76. doi:10.3847/1538-4357/abb5b8
- Panda, S., Martínez-Aldama, M. L., and Zajaček, M. (2019b). Current and future applications of Reverberation-mapped quasars in Cosmology. *Frontiers in Astronomy and Space Sciences* 6, 75. doi:10.3389/fspas.2019.00075
- Panda, S. and Marziani, P. (2023a). High Eddington quasars as discovery tools: current state and challenges. *Frontiers in Astronomy and Space Sciences* 10, 1130103. doi:10.3389/fspas.2023.1130103

- Panda, S. and Marziani, P. (2023b). Modeling the quasar spectra for super-Eddington sources. *Boletim da Sociedade Astronomica Brasileira* 34, 241–245. doi:10.48550/arXiv.2308.05830
- Panda, S., Marziani, P., and Czerny, B. (2019c). The Quasar Main Sequence Explained by the Combination of Eddington Ratio, Metallicity, and Orientation. *ApJ* 882, 79. doi:10.3847/1538-4357/ab3292
- Panda, S., Marziani, P., and Czerny, B. (2020b). Main trends of the quasar main sequence - effect of viewing angle. *Contributions of the Astronomical Observatory Skalnaté Pleso* 50, 293–308. doi:10.31577/caosp.2020.50.1.293
- Panda, S., Marziani, P., Czerny, B., Rodríguez-Ardila, A., and Pozo Nuñez, F. (2023b). Spectral Variability Studies in Active Galactic Nuclei: Exploring Continuum and Emission Line Regions in the Age of LSST and JWST. *Universe* 9, 492. doi:10.3390/universe9120492
- Panda, S., Pozo Nuñez, F., Bañados, E., and Heidt, J. (2024b). Probing the C IV Continuum Size–Luminosity Relation in Active Galactic Nuclei with Photometric Reverberation Mapping. *ApJL* 968, L16. doi:10.3847/2041-8213/ad5014
- Panda, S. and Śniegowska, M. (2024). Changing-look Active Galactic Nuclei. I. Tracking the Transition on the Main Sequence of Quasars. *ApJS* 272, 13. doi:10.3847/1538-4365/ad344f
- Pandey, A., Czerny, B., Panda, S., Prince, R., Jaiswal, V. K., Martínez-Aldama, M. L., et al. (2023). Broad-line region in active galactic nuclei: Dusty or dustless? *A&A* 680, A102. doi:10.1051/0004-6361/202347819
- Pandey, A., Martínez-Aldama, M. L., Czerny, B., Panda, S., and Zajaček, M. (2024). New theoretical Fe II templates for bright quasars. *arXiv e-prints*, arXiv:2401.18052doi:10.48550/arXiv.2401.18052
- Park, D., Barth, A. J., Ho, L. C., and Laor, A. (2022). A New Iron Emission Template for Active Galactic Nuclei. I. Optical Template for the H β Region. *ApJS* 258, 38. doi:10.3847/1538-4365/ac3f3e
- Peterson, B. M. (1988). Emission-Line Variability in Seyfert Galaxies. *PASP* 100, 18. doi:10.1086/132130
- Peterson, B. M. (1993). Reverberation Mapping of Active Galactic Nuclei. *PASP* 105, 247. doi:10.1086/133140
- Peterson, B. M., Ferrarese, L., Gilbert, K. M., Kaspi, S., Malkan, M. A., Maoz, D., et al. (2004). Central Masses and Broad-Line Region Sizes of Active Galactic Nuclei. II. A Homogeneous Analysis of a Large Reverberation-Mapping Database. *ApJ* 613, 682–699. doi:10.1086/423269
- Petrushevska, T., Leloudas, G., Ilić, D., Bronikowski, M., Charalampopoulos, P., Jaisawal, G. K., et al. (2023). The rise and fall of the iron-strong nuclear transient PS16dtm. *A&A* 669, A140. doi:10.1051/0004-6361/202244623
- Phillips, M. M. (1978a). Permitted Fe II Emission in Seyfert 1 Galaxies and QSOs I. Observations. *ApJS* 38, 187. doi:10.1086/190553
- Phillips, M. M. (1978b). Permitted Fe II emission in Seyfert 1 galaxies and QSOs. II. The excitation mechanism. *ApJ* 226, 736–752. doi:10.1086/156656
- Planck Collaboration, Aghanim, N., Akrami, Y., Ashdown, M., Aumont, J., Baccigalupi, C., et al. (2020). Planck 2018 results. VI. Cosmological parameters. *A&A* 641, A6. doi:10.1051/0004-6361/201833910
- Prince, R., Zajaček, M., Panda, S., Hryniewicz, K., Kumar Jaiswal, V., Czerny, B., et al. (2023). Wavelength-resolved reverberation mapping of intermediate-redshift quasars HE 0413-4031 and HE 0435-4312: Dissecting Mg II, optical Fe II, and UV Fe II emission regions. *A&A* 678, A189. doi:10.1051/0004-6361/202346738
- Pronik, V. I. and Chuvaev, K. K. (1972). Hydrogen lines in the spectrum of the galaxy Markaryan 6 during its activity. *Astrophysics* 8, 112–116. doi:10.1007/BF01002159
- Rakshit, S., Stalin, C. S., and Kotilainen, J. (2020). Spectral Properties of Quasars from Sloan Digital Sky Survey Data Release 14: The Catalog. *ApJS* 249, 17. doi:10.3847/1538-4365/ab99c5

- Ricci, C. and Trakhtenbrot, B. (2023). Changing-look active galactic nuclei. *Nature Astronomy* 7, 1282–1294. doi:10.1038/s41550-023-02108-4
- Richards, G. T., Lacy, M., Storrie-Lombardi, L. J., Hall, P. B., Gallagher, S. C., Hines, D. C., et al. (2006). Spectral Energy Distributions and Multiwavelength Selection of Type 1 Quasars. *ApJS* 166, 470–497. doi:10.1086/506525
- Riess, A. G., Casertano, S., Yuan, W., Macri, L. M., and Scolnic, D. (2019). Large Magellanic Cloud Cepheid Standards Provide a 1% Foundation for the Determination of the Hubble Constant and Stronger Evidence for Physics beyond Λ CDM. *ApJ* 876, 85. doi:10.3847/1538-4357/ab1422
- Riess, A. G., Filippenko, A. V., Challis, P., Clocchiatti, A., Diercks, A., Garnavich, P. M., et al. (1998). Observational Evidence from Supernovae for an Accelerating Universe and a Cosmological Constant. *AJ* 116, 1009–1038. doi:10.1086/300499
- Rigby, J., Perrin, M., McElwain, M., Kimble, R., Friedman, S., Lallo, M., et al. (2023). The Science Performance of JWST as Characterized in Commissioning. *PASP* 135, 048001. doi:10.1088/1538-3873/acb293
- Risaliti, G. and Lusso, E. (2015). A Hubble Diagram for Quasars. *ApJ* 815, 33. doi:10.1088/0004-637X/815/1/33
- Risaliti, G. and Lusso, E. (2019). Cosmological Constraints from the Hubble Diagram of Quasars at High Redshifts. *Nature Astronomy* 3, 272–277. doi:10.1038/s41550-018-0657-z
- Rodríguez-Ardila, A., Fonseca-Faria, M. A., Dias dos Santos, D., Panda, S., and Marinello, M. (2024). First Detection of Outflowing Gas in the Outskirts of the Broad-line Region in 1H 0707-495. *AJ* 167, 244. doi:10.3847/1538-3881/ad36bf
- Ross, N. P., Ford, K. E. S., Graham, M., McKernan, B., Stern, D., Meisner, A. M., et al. (2018). A new physical interpretation of optical and infrared variability in quasars. *MNRAS* 480, 4468–4479. doi:10.1093/mnras/sty2002
- Russell, H. N. (1914). Relations Between the Spectra and Other Characteristics of the Stars. *Popular Astronomy* 22, 275–294
- Sánchez-Sáez, P., Lira, H., Martí, L., Sánchez-Pi, N., Arredondo, J., Bauer, F. E., et al. (2021). Searching for Changing-state AGNs in Massive Data Sets. I. Applying Deep Learning and Anomaly-detection Techniques to Find AGNs with Anomalous Variability Behaviors. *AJ* 162, 206. doi:10.3847/1538-3881/ac1426
- Sarkar, A., Ferland, G. J., Chatzikos, M., Guzmán, F., van Hoof, P. A. M., Smyth, R. T., et al. (2021). Improved Fe II Emission-line Models for AGNs Using New Atomic Data Sets. *ApJ* 907, 12. doi:10.3847/1538-4357/abcaa6
- Savić, D., Goosmann, R., Popović, L. Č., Marin, F., and Afanasiev, V. L. (2018). AGN black hole mass estimates using polarization in broad emission lines. *A&A* 614, A120. doi:10.1051/0004-6361/201732220
- Schmidt, M. and Green, R. F. (1983). Quasar evolution derived from the Palomar bright quasar survey and other complete quasar surveys. *ApJ* 269, 352–374. doi:10.1086/161048
- Shapovalova, A. I., Popović, L. Č., Collin, S., Burenkov, A. N., Chavushyan, V. H., Bochkarev, N. G., et al. (2008). Long-term variability of the optical spectra of NGC 4151. I. Light curves and flux correlations. *A&A* 486, 99–111. doi:10.1051/0004-6361:20079111
- Shen, Y., Grier, C. J., Horne, K., Stone, Z., Li, J. I., Yang, Q., et al. (2024). The Sloan Digital Sky Survey Reverberation Mapping Project: Key Results. *ApJS* 272, 26. doi:10.3847/1538-4365/ad3936
- Shen, Y. and Ho, L. C. (2014). The diversity of quasars unified by accretion and orientation. *Nat* 513, 210–213. doi:10.1038/nature13712

- Shen, Y., Richards, G. T., Strauss, M. A., Hall, P. B., Schneider, D. P., Snedden, S., et al. (2011). A Catalog of Quasar Properties from Sloan Digital Sky Survey Data Release 7. *ApJS* 194, 45. doi:10.1088/0067-0049/194/2/45
- Śniegowska, M., Czerny, B., Bon, E., and Bon, N. (2020). Possible mechanism for multiple changing-look phenomena in active galactic nuclei. *A&A* 641, A167. doi:10.1051/0004-6361/202038575
- Śniegowska, M., Marziani, P., Czerny, B., Panda, S., Martínez-Aldama, M. L., del Olmo, A., et al. (2021). High Metal Content of Highly Accreting Quasars. *ApJ* 910, 115. doi:10.3847/1538-4357/abe1c8
- Śniegowska, M., Panda, S., Czerny, B., Savić, D., Martínez-Aldama, M. L., Marziani, P., et al. (2023). Spectropolarimetry and spectral decomposition of high-accreting narrow-line Seyfert 1 galaxies. *A&A* 678, A63. doi:10.1051/0004-6361/202243434
- Sulentic, J. and Marziani, P. (2015). Quasars in the 4D Eigenvector 1 Context: a stroll down memory lane. *Frontiers in Astronomy and Space Sciences* 2, 6. doi:10.3389/fspas.2015.00006
- Sulentic, J. W., Zwitter, T., Marziani, P., and Dultzin-Hacyan, D. (2000). Eigenvector 1: An Optimal Correlation Space for Active Galactic Nuclei. *ApJL* 536, L5–L9. doi:10.1086/312717
- Sun, J. and Shen, Y. (2015). Dissecting the Quasar Main Sequence: Insight from Host Galaxy Properties. *ApJL* 804, L15. doi:10.1088/2041-8205/804/1/L15
- Tananbaum, H., Avni, Y., Green, R. F., Schmidt, M., and Zamorani, G. (1986). X-Ray Observations of the Bright Quasar Survey. *ApJ* 305, 57. doi:10.1086/164228
- Trakhtenbrot, B., Arcavi, I., Ricci, C., Tacchella, S., Stern, D., Netzer, H., et al. (2019). A new class of flares from accreting supermassive black holes. *Nature Astronomy* 3, 242–250. doi:10.1038/s41550-018-0661-3
- Tsuzuki, Y., Kawara, K., Yoshii, Y., Oyabu, S., Tanabé, T., and Matsuoka, Y. (2006). Fe II Emission in 14 Low-Redshift Quasars. I. Observations. *ApJ* 650, 57–79. doi:10.1086/506376
- Vanden Berk, D. E., Richards, G. T., Bauer, A., Strauss, M. A., Schneider, D. P., Heckman, T. M., et al. (2001). Composite Quasar Spectra from the Sloan Digital Sky Survey. *AJ* 122, 549–564. doi:10.1086/321167
- Verner, E. M., Verner, D. A., Korista, K. T., Ferguson, J. W., Hamann, F., and Ferland, G. J. (1999). Numerical Simulations of Fe II Emission Spectra. *ApJS* 120, 101–112. doi:10.1086/313171
- Véron-Cetty, M. P., Joly, M., and Véron, P. (2004). The unusual emission line spectrum of I Zw 1. *A&A* 417, 515–525. doi:10.1051/0004-6361:20035714
- Vestergaard, M. and Wilkes, B. J. (2001). An Empirical Ultraviolet Template for Iron Emission in Quasars as Derived from I Zwicky 1. *ApJS* 134, 1–33. doi:10.1086/320357
- Wang, J., Wei, J. Y., and He, X. T. (2005). Variability of optical Fe II complex in narrow-line Seyfert 1 galaxy NGC 4051. *A&A* 436, 417–426. doi:10.1051/0004-6361:20042014
- Wang, J.-M., Qiu, J., Du, P., and Ho, L. C. (2014). Self-shadowing Effects of Slim Accretion Disks in Active Galactic Nuclei: The Diverse Appearance of the Broad-line Region. *ApJ* 797, 65. doi:10.1088/0004-637X/797/1/65
- Wang, J.-M., Songsheng, Y.-Y., Li, Y.-R., Du, P., and Zhang, Z.-X. (2020). A parallax distance to 3C 273 through spectroastrometry and reverberation mapping. *Nature Astronomy* 4, 517–525. doi:10.1038/s41550-019-0979-5
- Williams, P. R., Pancoast, A., Treu, T., Brewer, B. J., Barth, A. J., Bennert, V. N., et al. (2018). The Lick AGN Monitoring Project 2011: Dynamical Modeling of the Broad-line Region. *ApJ* 866, 75. doi:10.3847/1538-4357/aae086
- Wu, Q. and Shen, Y. (2022). A Catalog of Quasar Properties from Sloan Digital Sky Survey Data Release 16. *ApJS* 263, 42. doi:10.3847/1538-4365/ac9ead

- Yang, G., Boquien, M., Buat, V., Burgarella, D., Ciesla, L., Duras, F., et al. (2020). X-CIGALE: Fitting AGN/galaxy SEDs from X-ray to infrared. *MNRAS* 491, 740–757. doi:10.1093/mnras/stz3001
- Yang, J., Wang, F., Fan, X., Hennawi, J. F., Barth, A. J., Bañados, E., et al. (2023). A Spectroscopic Survey of Biased Halos in the Reionization Era (ASPIRE): A First Look at the Rest-frame Optical Spectra of $z \gtrsim 6.5$ Quasars Using JWST. *ApJL* 951, L5. doi:10.3847/2041-8213/acc9c8
- York, D. G., Adelman, J., Anderson, J., John E., Anderson, S. F., Annis, J., Bahcall, N. A., et al. (2000). The Sloan Digital Sky Survey: Technical Summary. *AJ* 120, 1579–1587. doi:10.1086/301513
- Zajaček, M., Czerny, B., Khadka, N., Martínez-Aldama, M. L., Prince, R., Panda, S., et al. (2024a). Effect of Extinction on Quasar Luminosity Distances Determined from UV and X-Ray Flux Measurements. *ApJ* 961, 229. doi:10.3847/1538-4357/ad11dc
- Zajaček, M., Panda, S., Pandey, A., Prince, R., Rodríguez-Ardila, A., Jaiswal, V., et al. (2024b). UV FeII emission model of HE 0413–4031 and its relation to broad-line time delays. *A&A* 683, A140. doi:10.1051/0004-6361/202348172
- Zamfir, S., Sulentic, J. W., Marziani, P., and Dultzin, D. (2010). Detailed characterization of $H\beta$ emission line profile in low- z SDSS quasars. *MNRAS* 403, 1759–1786. doi:10.1111/j.1365-2966.2009.16236.x
- Zeltny, G., Trakhtenbrot, B., Eracleous, M., Yang, Q., Green, P., Anderson, S. F., et al. (2024). Exploring Changing-look Active Galactic Nuclei with the Sloan Digital Sky Survey V: First Year Results. *ApJ* 966, 85. doi:10.3847/1538-4357/ad2f30
- Zu, Y., Kochanek, C. S., and Peterson, B. M. (2011). An Alternative Approach to Measuring Reverberation Lags in Active Galactic Nuclei. *ApJ* 735, 80. doi:10.1088/0004-637X/735/2/80